A Theoretical Approach to Pneumatic Muscle Mechanics

Francesco Sorge and Marco Cammalleri

***Abstract*— The mechanical response of pneumatic artificial muscles is analyzed assuming the inextensibility of the sheathing braids and taking into account the stress field inside the rubber bladder, which is regarded as a Mooney-Rivlin hyperelastic material. The end effects are simulated by heuristically profiling the meridian section. After estimating the constitutive parameters by traction tests on rubber specimens, the theoretical results are compared with experiments and a satisfactory accordance may be detected.**

LIST OF SYMBOLS

c	clearance ratio of sheath radius to bladder outer radius in undeformed state ($c = r_s / r_e$)
C	hyperelastic parameter defined by (11b) [N/mm^2]
C_1, C_2	Mooney-Rivlin hyperelastic constants [N/mm^2]
F_a, F_r, F_s, $F_{\text{tot.}}$	axial forces transmitted by air, rubber, sheath and whole muscle through cross-section [N]
l	invariable side of sheath lozenge [mm]
L	muscle length in undeformed state [mm]
L_h	invariable length of helical braid [mm]
n	number of lozenges around muscle circumference
p	pressure [N/mm^2]
r	radial coordinate [mm]
r_s	sheath radius in undeformed state [mm]
T	tensile force of single braid [N] ($T = \lvert \mathbf{T} \rvert$)
u_r	radial displacement component [mm]
z	axial coordinate [mm]
α	angle of helical braid
α_{critic}	limit value of α for $p_i \to \infty$
γ^*	slope of muscle meridian profile inside end region
ε	strain component
ζ	dimensionless axial coordinate inside end region ($\zeta = 1 - 2z/L'$, $\zeta = 0$ at the mid-span)
θ	angular coordinate
λ	stretch component ($\lambda = 1 + \varepsilon$)
ρ	square of radii ratio ($\rho = r^2/r_e^2$)
σ	stress component [N/mm^2]
ψ, $\psi_{\text{max.}}$	angular coordinate and angular half-width of lozenge ($-\psi_{\text{max.}} < \psi < \psi_{\text{max.}}$, see Fig. 2)
Δz	lozenge axial width inside end regions [mm]
$\Theta_{\text{tot.}}$	total winding angle of single braid
Λ	parameter defined by (7a)

Subscripts and superscripts

e, i	external and internal surfaces of rubber sub-layer
r, θ, z	cylindrical coordinates
m	binomial exponent of end region approximation
*	end region values
′	values in deformed state

F. Sorge is with the Dept. DICGIM, University of Palermo, 90128-Palermo, Italy (corresponding author, francesco.sorge@ unipa.it)

M. Cammalleri is with the Dept. DICGIM, University of Palermo, 90128-Palermo, Italy (marco.cammalleri@unipa.it)

I. INTRODUCTION

The pneumatic artificial muscle (PAM) is a simple and versatile bio-robotic actuator that can contract under load by inflating air into a cylindrical rubber chamber (bladder), which is wrapped by a double-helical braid mesh (sheathing): the inner bladder expands, reduces the helical slope and shortens the device length. The transverse expansion and the length decrease are mainly ruled by the geometry of the outer mesh, as the elastic elongation of the braids is negligible in comparison with the rubber compliance. The PAM's are very light and quite practical to replace defective human muscles (Fig. 1). Their response is non-linear and actually offers a very good simulation of the force-stretch relationship of biological muscles. The main PAM drawbacks are the need of a compressed air generator and the necessary softness of the rubber bladder, which subjects it to breakage danger.

Gaylord patented the use of the PAM device as an actuator [1] and McKibben was the first who applied it for orthopaedic purpose in the late fifties, whence it was named McKibben actuator. Nonetheless, the further definitive diffusion of the PAM's started near the end of the 20th century. Following the first theoretical model of Gaylord, several researchers analyzed the PAM mechanics for both static and dynamic loading histories. Among them, we recall the model of Chou and Hannaford [2], which neglected the rubber bladder thickness. Similar results were obtained by Tondu and Lopez [3] and by Tsagarakis and Caldwell [4], who improved the accuracy of the model taking into account the loss of the cylindrical shape due to the end effects. These and other similar models grounded their validity mainly on the empirical choice of some parameters for each single device, with the consequent obvious problems for a general applicability. The effects of the Coulombian friction among the braids was also considered in the analysis of the PAM fatigue resistance under repeated loading cycles. Klute and Hannaford [5] tried to improve the previous approaches by a new model based on the rubber hyperelastic description of Mooney and Rivlin [6,7]. Doumit et al. proposed a non-linear polynomial law for the elastomer response and a cone frustum representation of the PAM ends [8]. However, what often seems to be lacking in the various models is a definitive accordance of their results with the experimentation.

The present analysis considers the combined effects of the geometrical deformation of the external sheath and of the hyperelastic deformation of the tube material, which is here assumed incompressible and is described by a two-parameter Mooney-Rivlin law. The shape of the artificial muscle surface near the end fixtures is expressed by an algebraic

Figure1. Example of pneumatic artificial muscle

relation among the cylindrical coordinates, whose coefficients are fixed by heuristic criteria. The hyperelastic constitutive parameters are derived by traction tests on rubber specimens. The influence of some possible initial clearance between the sheath and the bladder in rest conditions is carefully analyzed as well. On the whole, the accordance of the theoretical diagrams with experiments appears sufficiently acceptable and somehow meets the authors' effort to propose a new reliable model based on a relatively simple formulation.

II. Mechanical Response of Pneumatic Muscles

A. General Theory

Indicate the undeformed and deformed states without superscripts and with primes respectively and the external and internal surfaces of the rubber tube with the subscripts *e* and *i*. Neglect the end effects at first and consider one single lozenge formed by the double-helical sheathing together with the underlying element of the rubber bladder, as in Fig. 2. All the braids are subject to the same tensile force T, lie upon a cylindrical surface of radius r'_e and are inclined of the same angle α' with respect to the cross-section (helical angle). As the sheath is very closely woven, the effect of the forces T on the rubber is equivalent to a uniform radial pressure p_e acting on the bladder from the outside. Nevertheless, some attention must be paid to the influence of the rubber penetration into the interstices among the sheath threads, which may be assumed to reduce the effective thickness of the inner bladder to a certain fraction of the whole real thickness. Here, it is supposed that each element of the mixed rubber-sheath outer layer, which surrounds and presses the rubber effective inner layer, is subject to the only forces T and to the radial pressure p_e exerted by the rubber inner layer.

Integrating the elementary pushes of the uniform pressure p_e throughout the external surface of the rubber element of Fig. 2, the radial equilibrium of the rubber-sheath outer layer implies that

$$4T\cos\alpha'\sin\psi_{\max.} = 2p_e r'_e l \sin\alpha' \int_{-\psi_{\max.}}^{\psi_{\max.}} \cos\psi \, d\psi$$

whence $T = p_e l r'_e \tan\alpha'$. As the number of lozenges around a cylinder slice of width $2l\sin\alpha'$ is $n = \pi r'_e/(l\cos\alpha')$, the total tensile axial force transmitted by the sheath layer through the cross-section is $F_s = 2nT\sin\alpha' = 2\pi p_e r'^2_e \tan^2\alpha'$, as may be inferred by replacing T and n. On the other hand, the compressive force exerted by the air through the cross-section hole is $F_a = -\pi p_i r'^2_i$.

Indicating the lengths of a single helical braid and of the whole pneumatic muscle with L_h and L' respectively ($L' = L$

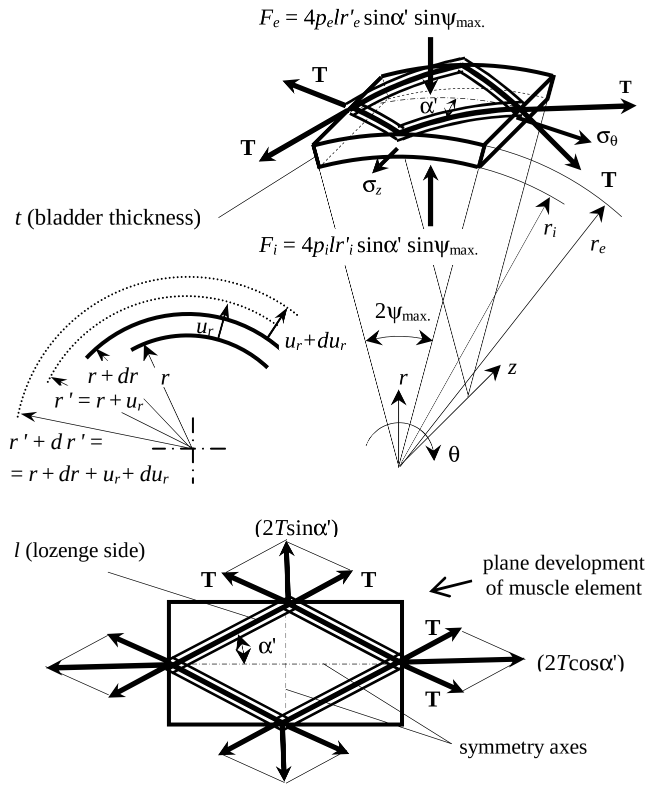

Figure 2. Element of rubber bladder plus sheath, corresponding to one single lozenge. F_e and F_i are the resultant radial forces exerted on the external and internal curved surfaces of the rubber element

in the undeformed state, where $\alpha' = \alpha$), one has the self-evident relations $L_h \sin\alpha' = L'$ and $L_h \cos\alpha' = r'_e\Theta_{tot.}$, where $\Theta_{tot.}$ is the total winding angle of the braid. Therefore, minding that L_h is constant by hypothesis and assuming adherence conditions between the sheath and the rubber tube, the longitudinal and circumferential stretches of the rubber at the outer radius are given by

$$\lambda_z = \frac{L'}{L} = 1 + \varepsilon_z = \frac{\sin\alpha'}{\sin\alpha}$$
$$\lambda_{\theta e} = \frac{r'_e}{r_e} = 1 + \varepsilon_{re} = c\frac{\cos\alpha'}{\cos\alpha} \qquad (1a,b)$$

where the subscript *e* was omitted in the *z* direction because the axial stretch is uniform throughout the cross-section. Moreover: r' and r indicate the radial coordinates of a generic rubber layer in the deformed spatial state (Eulerian reference) and in the undeformed material state (Lagrangian reference); $c = r_s/r_e \geq 1$ is a clearance parameter, equal to the ratio of the sheath and tube radii in rest conditions; the ε's are strain components. Notice that the equilibrium must be analyzed using the actual spatial coordinates in the deformed state, whereas the stretches must be measured from the material undeformed state ($\lambda_\theta = r'/r$). It is worthy of notice that, if some initial clearance exists at rest between the sheath and the bladder, i. e. $c > 1$, this clearance may be retrieved either by stretching the muscle with zero inner pressure, as the cross-section of the tube shrinks much more slowly than the radius decrease of the sheath, or by insufflating compressed air into the muscle and keeping its length constant. After the clearance retrieval, one has $\lambda_{\theta e} = (r_s / r_e)(r'_e / r_s) = c \cos\alpha' / \cos\alpha$. Here, it is to be noted that the retrieval of some possible clearance is obtained quite soon in practical cases, applying an even small load.

Therefore, the sum of the sheath and air forces may be expressed in the form

$$F_s + F_a = \pi\left(\frac{2 p_e r_e^2 c^2 \sin^2\alpha'}{\cos^2\alpha} - p_i r_i^2 \lambda_{\theta i}^2\right) \tag{2}$$

and, neglecting the bladder influence ($r_e = r_i$, $p_e = p_i$, $c = 1$, $\lambda_{\theta i} = \lambda_{\theta e} = \cos\alpha'/\cos\alpha$), Equation (2) would return the conventional model of Chou and Hannaford [2].

The search for the stress and deformation distributions inside the bladder requires applying the local equilibrium equations and formulating proper constitutive laws for the rubber. Considering that the directions r, θ and z of Fig. 2 are principal due to the axial symmetry, and indicating the radial displacement from the undeformed state with u_r, one has

$$\begin{aligned} r' &= r + u_r = \lambda_\theta r \quad \rightarrow \quad \varepsilon_\theta = \frac{u_r}{r} \\ dr' &= dr + du_r = \lambda_r dr \quad \rightarrow \quad \varepsilon_r = \frac{du_r}{dr} \end{aligned} \tag{3a,b}$$

where the stretches $\lambda_r = (1 + \varepsilon_r)$, $\lambda_\theta = (1 + \varepsilon_\theta)$ and $\lambda_z = (1 + \varepsilon_z)$ are independent of the axial coordinate z and are subject to the rubber incompressibility condition

$$\lambda_r \lambda_\theta \lambda_z = (1+\varepsilon_r)(1+\varepsilon_\theta)(1+\varepsilon_z) = 1 \tag{4}$$

Equations (3a,b) give place to

$$\frac{d\varepsilon_\theta}{dr} = \frac{\varepsilon_r - \varepsilon_\theta}{r} \quad \rightarrow \quad \frac{d\lambda_\theta}{dr} = \frac{\lambda_r - \lambda_\theta}{r} \tag{5a,b}$$

while, in the absence of body forces, the radial equilibrium equation may be simply expressed by

$$\frac{d\sigma_r}{dr'} = \frac{\sigma_\theta - \sigma_r}{r'} \quad \rightarrow \quad \frac{d\sigma_r}{dr} = \left(\frac{\lambda_r}{\lambda_\theta}\right)\frac{\sigma_\theta - \sigma_r}{r} \tag{6a,b}$$

Thus, we have collected three equations (4, 5b, 6b) in the five unknowns λ_r, λ_θ, σ_r, σ_θ, σ_z, while λ_z is given by Eq. (1a) and is independent of r. The extra equations needed for the closure of the mathematical problem may be written by properly specifying the material properties of the rubber. Yet, regardless of the rubber constitutive equations, the stretch equations (4-5b) can be integrated across the bladder thickness. Putting for brevity

$$\Lambda = \lambda_{\theta e}^2 \lambda_z - 1 \qquad \rho = \frac{r^2}{r_e^2} \qquad \rho_i = \frac{r_i^2}{r_e^2} \tag{7a,b,c}$$

the integration gives

$$\lambda_\theta^2 = \frac{\rho + \Lambda}{\rho \lambda_z} \quad \text{and} \quad \lambda_r^2 = \frac{1}{\lambda_\theta^2 \lambda_z^2} = \frac{\rho}{\lambda_z[\rho + \Lambda]} \tag{8a,b}$$

whence $\lambda_{\theta i}^2 = (\rho_i + \Lambda)/(\rho_i \lambda_z)$ and, accounting for (1b) and (7a), Equation (2) may be changed into

$$\frac{F_s + F_a}{\pi r_s^2} = \frac{2 p_e \sin^2\alpha' - p_i \cos^2\alpha'}{\cos^2\alpha} + \frac{p_i}{\lambda_z c^2}(1 - \rho_i) \tag{9}$$

where $c = 1$ and $r_s = r_e$ for zero initial clearance.

B. Constitutive Laws of the Rubber Bladder

As already emphasized, the large deformation of the pneumatic muscle requires a careful distinction between spatial and material coordinates and involves the choice of a non-Hookean definition of the rubber behaviour. Here, a Mooney-Rivlin model with the two material constants C_1 and C_2 will be applied relying on its excellent fit with the response of many elastomer materials. For incompressible solids, such as rubber, one can define the stress-stretch relations, apart from a hydrostatic stress, in the form:

$$\begin{aligned} \sigma_\theta - \sigma_r &= 2C_1\left(\lambda_\theta^2 - \lambda_r^2\right) + 2C_2\left(\frac{1}{\lambda_r^2} - \frac{1}{\lambda_\theta^2}\right) \\ \sigma_z - \sigma_r &= 2C_1\left(\lambda_z^2 - \lambda_r^2\right) + 2C_2\left(\frac{1}{\lambda_r^2} - \frac{1}{\lambda_z^2}\right) \end{aligned} \tag{10a,b}$$

Transforming (6b) into

$$\frac{d\sigma_r}{d\rho} = \left(\frac{\lambda_r}{\lambda_\theta}\right)\frac{\sigma_\theta - \sigma_r}{2\rho}$$

replacing the right hand of (10a) and using the functions $\lambda_\theta(\rho)$ and $\lambda_r(\rho)$ given by (8a,b), it is possible to integrate for $\sigma_r(\rho)$ and, imposing the boundary condition $\sigma_r = -p_i$ for $\rho = \rho_i$, obtain:

$$\begin{aligned} \sigma_r &= -p_i + C\left[\frac{\Lambda}{\Lambda + \rho_i} - \frac{\Lambda}{\Lambda + \rho} - \ln\left(\frac{1 + \dfrac{\Lambda}{\rho}}{1 + \dfrac{\Lambda}{\rho_i}}\right)\right] \\ C &= \frac{C_1 + C_2 \lambda_z^2}{\lambda_z} \end{aligned} \tag{11a,b}$$

The two other principal stresses σ_θ and σ_z are very easily obtained by (10a,b), using (4), (8a,b) and (11a,b):

$$\begin{aligned} \sigma_\theta &= \sigma_r + 2C\left(\frac{\rho + \Lambda}{\rho} - \frac{\rho}{\rho + \Lambda}\right) \\ \sigma_z &= \sigma_r + 2\left(\frac{C_1 \rho \lambda_z}{\rho + \Lambda} + C_2\right)\left[\frac{(\rho + \Lambda)\lambda_z}{\rho} - \frac{1}{\lambda_z^2}\right] \end{aligned} \tag{12a,b}$$

Applying the outer boundary condition, $\sigma_r = -p_e$ for $\rho = 1$, one gets

$$p_e - p_i = C\left[\frac{\Lambda}{\Lambda + 1} - \frac{\Lambda}{\Lambda + \rho_i} - \ln\left(\frac{1 + \dfrac{\Lambda}{\rho_i}}{1 + \Lambda}\right)\right] \tag{13}$$

which relation permits calculating p_e and $T = cp_e l r_e \sin\alpha'/\cos\alpha$ in dependence on p_i and on the muscle deformation. Moreover, using (3a,b), the force transmitted by the rubber tube is given by

$$F_r = 2\pi\int_{r_i'}^{r_e'}\sigma_z r' dr' = \left(\pi r_e^2/\lambda_z\right)\int_{\rho_i}^{1}\sigma_z d\rho$$

and, replacing σ_z by (12b), integrating and adding $F_r/\pi r_s^2$ to Eq. (9), one obtains at last, after some algebra,

$$\begin{aligned}\frac{F_{\text{tot.}}}{\pi r_s^2} &= \frac{F_s+F_a+F_r}{\pi r_s^2} = p_i\left(\frac{3\sin^2\alpha'-1}{\cos^2\alpha}\right)+\\ &2\lambda_z^2 C\tan^2\alpha\left[\frac{\Lambda}{(\Lambda+1)}-\frac{\Lambda}{(\Lambda+\rho_i)}-\ln\left(\frac{1+\dfrac{\Lambda}{\rho_i}}{1+\Lambda}\right)\right]-\\ &\frac{1}{\lambda_z c^2}\Bigg\{\left(C+2C_2\Lambda\lambda_z\right)\ln\rho_i-\\ &\left[C(2\Lambda+1)-\frac{2C_1\Lambda}{\lambda_z}\right]\ln\left(\frac{\Lambda+\rho_i}{\Lambda+1}\right)-\\ &\left[\frac{C\Lambda}{(\Lambda+\rho_i)}+2(C_1\lambda_z+C_2)\left(\lambda_z-\frac{1}{\lambda_z^2}\right)\right](1-\rho_i)\Bigg\}\end{aligned} \tag{14}$$

Equation (14) indicates a linear affine relation between $F_{\text{tot.}}$ and p_i for fixed helical angle α', i.e. for fixed λ_z and Λ. Moreover, the pressure p_i may be seen to diverge for $\sin^2\alpha' = 1/3$ ($\alpha'_{\text{critic}} \cong 35°16'$), whence the limit axial contraction of the muscle is $L(1-\lambda_{z,\text{min.}}) = L[1-1/(\sqrt{3}\sin\alpha)]$ and is as larger as longer is the muscle and as larger is the initial helical angle α. Moreover, replacing the expressions (1a,b) into (7a), one observes that α'_{critic} yields also a maximum of Λ:

$$\Lambda = c^2\frac{\sin\alpha'\cos^2\alpha'}{\sin\alpha\cos^2\alpha}-1 \;\rightarrow\; \frac{d\Lambda}{d\alpha'} = c^2\frac{\cos\alpha'\left(1-3\sin^2\alpha'\right)}{\sin\alpha\cos^2\alpha} \tag{15a,b}$$

The operative conditions of a typical pneumatic muscle always involve α' values rather larger than α'_{critic}, whence Λ is a decreasing function of α' and, inflating air, α' decreases but never reaches the critical value. Notice also that the pressure jump $p_e - p_i$ may be regarded as a function of the only stretch λ_z by (13), where $\Lambda = \Lambda(\alpha') = \Lambda(\lambda_z)$.

The previous results can be simplified in the realistic hypotheses of a very thin bladder and $c = 1$. For $t = r_e - r_i \rightarrow 0$, $\rho_i \cong 1 - 2t/r_e$, where t is the thickness, and Equations (13) and (14) may be changed into simpler approximate equations, linear and linear affine in t respectively:

$$p_e - p_i = -2C\frac{t}{r_e}\left(1-\frac{1}{\lambda_{\theta e}^4\lambda_z^2}\right) \tag{16}$$

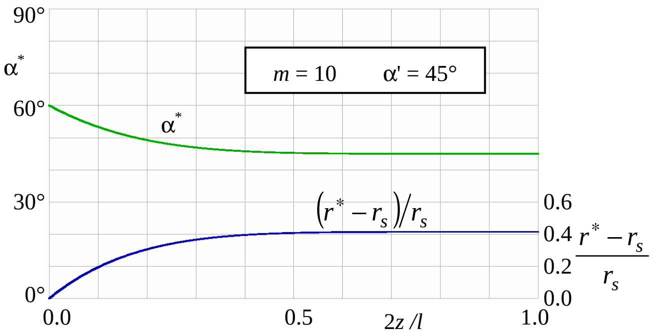

Figure 3. End trend of braid helical slope and muscle radius.

$$\begin{aligned}\frac{F_{\text{tot.}}}{\pi r_e^2} = p_i\left(\frac{3\sin^2\alpha'-1}{\cos^2\alpha}\right)+4\frac{t}{r_e}\Bigg[\frac{C_1}{\lambda_z}\left(\lambda_z^2-\frac{1}{\lambda_{\theta e}^2\lambda_z^2}\right)+\\ \frac{C_2}{\lambda_z}\left(\lambda_{\theta e}^2\lambda_z^2-\frac{1}{\lambda_z^2}\right)-C\lambda_z^2\tan^2\alpha\left(1-\frac{1}{\lambda_{\theta e}^4\lambda_z^2}\right)\Bigg]\end{aligned} \tag{17}$$

C. End Effects

The following simple model may successfully simulate the muscle end shape, after the possible clearance retrieval between the sheath and the bladder. Denoting the variables with the superscript $(\ldots)^*$ in the end regions, the number of braids of each helical formation is given by $n = \pi r^*/(l\cos\alpha^*)$, whence the radius r^* is proportional to $\cos\alpha^*$ ($r^*/r_s = \cos\alpha^*/\cos\alpha$). Assume that the sheath is cylindrical in the undeformed state and that the change of the radius r^* along a meridian section of the deformed muscle may be expressed by the binomial law $r^*(z) = r_e' - (r_e' - r_s)(1 - 2z/L')^m$, where m is a suitably large exponent, L' and r' are the muscle length and the mid-span radius under load and $z = 0$ at the extremity. Diagrams obtainable for $r^*(z)$ and $\alpha^*(z)$ turn out to be very realistic, with a rapid trend to the mid-span values r_e' and α' provided that m is sufficiently large (see Fig. 3). Of course, the choice of m should be based on experimental resemblance concepts.

Indicating the axial extent of each single lozenge with $\Delta z^* = 2l\sin\alpha^*\cos\gamma^*$, where γ^* is given by

$$\tan\gamma^* = \frac{dr^*}{dz} = \frac{2m}{L'}\left(r_e'-r_s\right)\left(1-\frac{2z}{L'}\right)^{m-1}$$

the axial width of a muscle slice associated with a lozenge collar is

$$\Delta z^* = \Delta z\frac{\sqrt{1-\cos^2\alpha^*}}{\sin\alpha\sqrt{1+\tan^2\gamma^*}}$$

where $\Delta z = 2l\sin\alpha$ is the slice axial width in cylindrical unloaded conditions ($\gamma^* = 0$, $\alpha^* = \alpha$). Therefore, letting $n \rightarrow \infty$, $\Delta z \rightarrow dz$, $\Delta z^* \rightarrow dz^*$ as the sheath is very densely woven, solving with respect to dz, putting $\zeta = 1 - 2z/L'$ and integrating, one gets

$$\int_0^{L/2} dz = \frac{L}{2} = \frac{L'\sin\alpha}{2}\int_0^1 \sqrt{\frac{1+\left(\frac{L}{L'}\right)^2\left(\frac{2mr_s}{L}\right)^2\left(\frac{\cos\alpha'}{\cos\alpha}-1\right)^2\zeta^{2m-2}}{1-\cos^2\alpha\left[\frac{\cos\alpha'}{\cos\alpha}-\left(\frac{\cos\alpha'}{\cos\alpha}-1\right)^2\zeta^m\right]^2}}\,d\zeta$$

Fixing the tube geometric parameter $2mr_s/L$, this equation has to be solved for the elongation or contraction ratio L'/L for each level of the inflation ratio $\cos\alpha'/\cos\alpha$, where α' is the braid slope at the mid-span, or also, approximately, inside a middle region centred on the mid-span, and is the same that was used in the previous sub-sections. This calculation may be quickly carried out by some iterative procedure and yields the muscle contraction $L - L'$ depending on the load and on the air pressure.

For large diameters of the end fixtures, the PAM mid-span radius may happen to be smaller than the fixture radius in rest conditions. In this case, the radius r_s has to be replaced by r_{fixture} in the previous binomial law and the ensuing formulas must consequently be corrected.

III Identification of Constitutive Parameters

When performing experimental traction tests on prismatic rubber specimens, only the stress in the traction direction is different from zero, say σ_z, while the principal stretches on the plane orthogonal to z are equal to each other by the Cartesian counterpart of (10a) and the incompressibility of the rubber implies that $\lambda_x = \lambda_y = 1/\sqrt{\lambda_z}$. Putting $\sigma_z = \sigma$, $\lambda_z = \lambda = 1 + \varepsilon$, the Cartesian form of (10b) gives

$$\sigma = 2\left(C_1 + \frac{C_2}{\lambda}\right)\left(\lambda^2 - \frac{1}{\lambda}\right) \tag{18}$$

A rubber specimen of sizes 30×10×0.78 mm (bladder of the following section) was subject to axial traction on a test machine INSTRON series IX for soft materials in the laboratories of the DICGIM of the University of Palermo. The strain was firstly increased to the level 50% with a slower velocity (1 mm/minute) and then with a much larger velocity until its breakage (100 mm/minute). During the test, measures of the traction force and of the vice displacement were taken with a frequency of 5 pt/s. The stress value was obtained from the force taking into account the section restriction, which was inversely proportional to the elongation due to the material incompressibility. The results are shown in the Figures 4a, for the whole test and 4b for the slow loading phase. These figures point out the non-linear nature of the material response. The two constitutive parameters were derived imposing the slope $d\sigma/d\varepsilon = 6(C_1 + C_2)$ for $\varepsilon \to 0$ and the best fit in the region of interest ($\varepsilon < 50\%$). Processing the numerical data and comparing with Eq. (18), the material constants were estimated and rounded to: $C_1 = -\,0.05$ N/mm^2, $C_2 = 0.5$ N/mm^2.

It is noteworthy that the Mooney-Rivlin uniaxial model may justify the very rapid retrieval of some possible clearance between the bladder and the sheath when loading the muscle at zero pressure. Indicating the braid angle with α_s, the sheath radius contraction is given by $\lambda_{\theta,\text{sheath}} =$

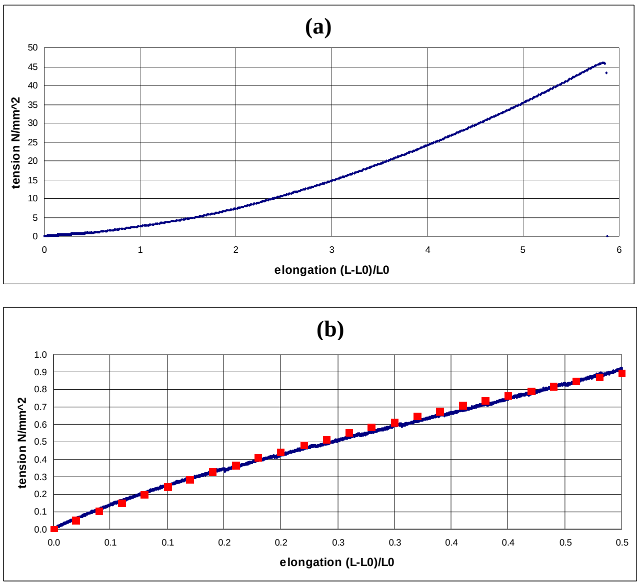

Figure 4 a,b. Experimental results from traction test on rubber specimen. Red dots: Mooney-Rivlin, $2C_1 = -0.1$, $2C_2 = 1$.

$\cos\alpha_s/\cos\alpha$, whereas the tube radius shrink is $\lambda_{\theta,\text{rubber}} = 1/\sqrt{\lambda_z} = \sqrt{\sin\alpha/\sin\alpha_s}$. The ratio of these two quantities is

$$\lambda_{\theta,\text{sheath}}/\lambda_{\theta,\text{rubber}} = \sqrt{\left(\sin\alpha_s\cos^2\alpha_s\right)/\left(\sin\alpha\cos^2\alpha\right)}$$

and, for fixed α, is a decreasing function of α_s, as was observed by Eqs. (15a,b), indicating that the sheath restriction pursues and reaches quickly the tube restriction.

IV Experimental Comparison

The theory of the previous sections was compared with some experimental results for a pneumatic artificial muscle, as they were reported in a degree thesis of the DEIM of the University of Palermo [9]. In rest conditions, the length, diameter and thickness of the tube were 120 mm, 22 mm and 0.78 mm respectively, while the helical angles were 65°. The experimental tests had been planned by a gradual increase of the internal pressure for several fixed levels of the loading force.

Figure 5 shows, in red, the experimental diagrams of the PAM contraction from the zero pressure configuration. As observable, some small growth of the pressure is generally required before the muscle starts contracting. Then all plots show a ramp, which corresponds to the practical operation of the PAM, and a final trend to a sort of saturation contraction, which corresponds to the previously mentioned critical slope α_{critic}. The contracting behaviour was simulated by the theory of the previous sections, taking into consideration the hyperelastic properties of the rubber and the end effects, ignoring the elongation of the nylon threads and assuming that an external fraction of the rubber thickness was merged into the sheath (50%, i. e. $t \cong 0.4$ mm), due to the rubber penetration into the interstices among the threads. In particular, the theoretical results were calculated using (14), and are shown in light blue in Fig. 5a. An acceptable agreement may be observed, save for low loads, with a

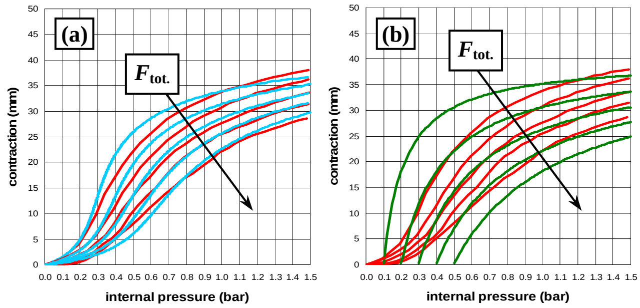

Figure 5 a,b. Plots of contraction vs internal pressure for various loads: $F_{tot.}$ = 30, 60, 90, 120, 150 N. Red: experiments. Light blue: present theory. Green: conventional theory (zero thickness rubber membrane) Data: α = 65°, C_1 = –0.05, C_2= 0.5, c = 1, $t_{eff.}$ / $t_{tot.}$ = 0.5, m = 6

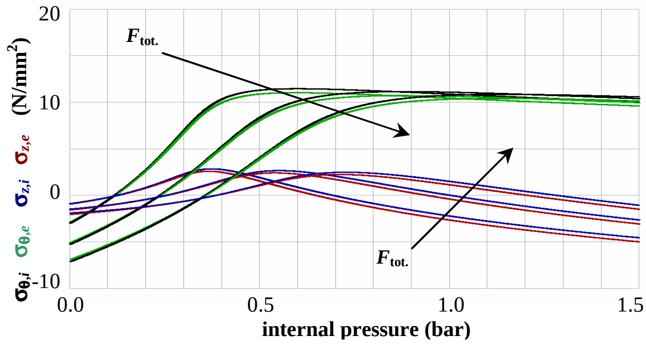

Figure 6. Plots of circumferential tension (black: inner radius; green: outer radius) and axial tension (blue: inner radius; red: outer radius) vs internal pressure for various loads. $F_{tot.}$ = 50, 100, 150 N (other data like in Fig. 4)

maximum error of roughly 10% in the main applicative region of the curve ramps. This points out the applicability of the present model to the PAM design or else to the performance prediction of some existing PAM. Figure 5b shows, in green, the results by the conventional model of references [1,2], which considers the bladder as a membrane with zero thickness and may be obtained by Eqs. (16-17) imposing $t = 0$. This model is generally used in literature but, as observable, the results are rather far from the experiments and moreover, they denote the impossibility of capturing the muscle behaviour for very low pressure values, as $\sin\alpha'$ should have to diverge for $p_i \rightarrow 0$ and non-zero $F_{tot.}$, differently from the present theory. The results obtainable by other much more complex models of the recent past, which also take into consideration the thickness and the non-linear elasticity of the bladder, should be expected in a rough intermediate position between the green and red curves, similarly to the experimental-theoretical accordance of the tests presented by their authors.

In parallel, the present theoretical model permits also detecting the stress distribution inside the rubber, which may be useful to check some possible critical state of the PAM working conditions in terms of rubber resistance. As an example, Figure 6 shows the diagrams of the outer and inner values of the stresses σ_θ and σ_z, between whose levels such two stresses can be found to vary in a monotonic roughly linear manner. Obviously, the radial stress σ_r varies between $-p_i$ and $-p_e$. As observable, the overall stress state of the cross-section plane is in part compressive and in part tractive, depending on the operative conditions, and is slightly higher at the inner surface of the tube.

V CONCLUSION

The mechanical behaviour of a pneumatic artificial muscle may be simulated by a relatively simple theoretical model assuming the inextensibility of the external sheathing fibres and modelling the inner bladder by a two-parameter Mooney-Rivlin material with a properly chosen effective thickness. The non-cylindrical muscle shape near the extremities may be taken into consideration by simple algebraic relations and the changes of the muscle response due to some possible initial clearance between the two structural components may also be taken into account. The analysis includes the estimate of the stress and deformation distribution inside the rubber tube, whose mechanical resistance has to be considered as the most critical with regard to the device breakage. Calculating the constitutive parameters of the rubber tube by traction tests, the theoretical results can be compared with the experiments, showing a fine accordance despite some uncertainty in the determination of many physical quantities of the actuator.

ACKNOWLEDGMENT

The authors are grateful to Prof. F. D'Ippolito of the DEIM, University of Palermo, Italy, for providing them with experimental results.

REFERENCES

[1] R. H. Gaylord, “Fluid actuated motor system and stroking device,” U.S. Patent 2844126, July 22, 1958.

[2] C. P. Chou and B. Hannaford, “Measurement and modelling of McKibben pneumatic artificial muscles,” *IEEE Trans. Robot. Autom.*, vol. 12, no. 1, Feb. 1996, pp. 90–102.

[3] B. Tondu and P. Lopez, “Modelling and control of McKibben artificial muscle robot actuators,” *IEEE Control Syst. Mag.*, vol. 20, no. 2, Apr. 2000, pp. 15–38.

[4] N. Tsagarakis and D. G. Caldwell, “Improved modelling and assessment of pneumatic muscle actuators,” in *Proc. Int. Conf. Robot. Autom.*, 2000, vol. 4, pp. 3641–3646.

[5] G. K. Klute and B. Hannaford, “Accounting for elastic energy storage in McKibben artificial muscle actuators,” *J. Dyn. Syst., Meas., Control*, vol. 122, no. 2, pp. 386–388, 2000.

[6] M. Mooney, “A theory of large elastic deformation”, Journal of Applied Physics, vol. 11, n. 9, 1940, pp. 582–592.

[7] R. S. Rivlin, “Large elastic deformations of isotropic materials. IV. Further developments of the general theory, Philosophical Transactions of the Royal Society of London. Series A, Mathematical and Physical Sciences, 241(835), 1948, pp. 379–397.

[8] M. Doumit, A. Fahim and M. Munro, “Analytical Modelling and Experimental Validation of the Braided Pneumatic Muscle”, IEEE Trans. on Robotics, vol. 25, n. 6, Dec. 2009, pp. 1282–1291.

[9] G. Cangemi, “Caratterizzazione di muscoli artificiali pneumatici per applicazioni robotiche” (in Italian), degree thesis, F. D’Ippolito supervisor, DEIM, University of Palermo, Italy, 2011.